Supporting Information for

Mechanism of Hydrogen Storage on Fe_3B

Zhao Ding [a,b], Hao Li [c], Ge Yan [d], Weijie Yang *[d], Zhengyang Gao [d], Wenhui Ma [e] and Leon Shaw [b]

[a] The State Key Laboratory of Refractories and Metallurgy, Institute of Advanced Materials and Nanotechnology, Wuhan University of Science and Technology, Wuhan, China

[b] Department of Mechanical, Materials and Aerospace Engineering, Illinois Institute of Technology, Chicago, Illinois, USA

[c] Department of Physics, Technical University of Denmark, 2800 Kongens Lyngby, Denmark

[d] School of Energy, Power and Mechanical Engineering, North China Electric Power University, Baoding, China

[e] Faculty of Metallurgical and Energy Engineering, Kunming University of Science and Technology, Kunming, China

* Corresponding Author: yangwj@ncepu.edu.cn

1. Experimental Section

All the calculations were conducted by Vienna *ab initio* simulation package (VASP 5.4.4) with projector-augmented-wave (PAW) potential [1] and Perdew-Burke-Ernzerhof (PBE) functional,[2, 3] based on DFT methods.[4-8] To model the Fe_3B structures, an optimized unit cell containing 24 Fe and 8 B atoms was employed, while the vacuum layer was set as 15 Å to prevent the effect of mirror images. [9, 10] The lattice parameters were calculated (a=9.70 Å, b=7.01 Å, c=19.23 Å). Six Fe layers was established and the topmost three atomic layers were allowed to relax. The cutoff energy of the plane wave basis set was set as 500 eV, which was used for relaxation structures.[11] Considering the computational cost and accuracy, a 5×5×1 Γ-centered *k*-point grid was used and the maximum ionic force was less than 0.02 eV/Å[12] with the Gaussian smearing set to 0.05 eV.[13] The convergence criteria of the self-consistent electron iteration was set to 10^{-5} eV. In detail, the ISPIN parameter was set to 2 for spin-polarized calculations.[14] Atomic charges and electrons transfer were analyzed based on the Bader charge method.[15] The H_2 coverage was defined as the ratio of the number of adsorbed H_2 to the maximum number of adsorbed H_2 on Fe_3B surface.[16]

All the possible surfaces were considered for hydrogen storage, and the surface energies were employed to determine the stability of the Fe_3B surface, which was calculated as follows:

$$E_{surf} = (E_{slab} - nE_{bulk})/2A \tag{S1}$$

where $E_{slab}$and E_{bulk} respectively represent the energies of the slab and the bulk after full relaxation; n is the number of primitive cells; A is the surface area.

The surface energies of (001), (010), and (100) are calculated to be 0.17, 0.21, and 0.21 eV, respectively. Therefore, (001) is the most stable crystal surface among these due to its lowest surface energy. Furthermore, we tested the model with five layers which has the thickness of 2.47 Å. The model with five layers had the adsorption energy of -0.98 eV, similar to the model with six layers (-1.00 eV). Therefore, the Fe_3B models with six layers were selected in this work.

The adsorption energy (E_{ads}) of H_2 on Fe_3B, which was used to measure the adsorption strength between the adsorbent and adsorbate, was calculated as follows: [17]

$$E_{ads} = E_{Fe_3B + nH_2} - E_{Fe_3B + (n-1)H_2} - E_{H_2} \quad (n = 1 - 6) \tag{S2}$$

where $E_{Fe_3B + nH_2}$, $E_{Fe_3B + (n-1)H_2}$, and E_{H_2} represent the total energy of Fe_3B with *n* H_2, Fe_3B with (*n*-1) H_2, and H_2 gas, respectively. Theoretically, the more negative of the E_{ads}, the more stable the adsorption interaction. Noted if the absolute value is larger than 0.5 eV, the adsorption is considered as chemisorption.

ΔG_{ads} of the adsorption of 1-6 H_2 on Fe_3B were calculated for thermodynamic analysis through the following equations:

$$\Delta G_{ads} = G_{Fe_3B + nH_2} - G_{Fe_3B + (n-1)H_2} - G_{H_2} \quad (n = 1 - 6) \tag{S3}$$

$$G_{gas} = E_{ele} + ZPE + RT - TS \tag{S4}$$

$$G_{solid} = E_{ele} + ZPE - TS \tag{S5}$$

where $G_{Fe_3B + nH_2}$, $G_{Fe_3B + (n-1)H_2}$, and G_{H_2} represents the Gibbs free energy of Fe_3B with *n* H_2, Fe_3B with (*n*-1) H_2, and H_2 gas, respectively. E_{ele} is the ground-state electron energy, eV; *ZPE* is the zero-point energy correction, eV; *R* is the gas constant, 8.314 $J \cdot mol^{-1} \cdot k^{-1}$; T is the temperature, K; *S* is the entropy obtained from vibrational frequency.

We also discussed the impact of termination of the surfaces. We found that that the Fe-termination is more favorable for hydrogen activation and adsorption due to the exposure of active Fe sites. Therefore, the selected surfaces were terminated by Fe.

2. Effect of Fe_3B surface on the H_2 adsorption

To further analyze the effect of Fe_3B surface on H_2 adsorption, the PDOS profiles of the first to sixth H_2 on Fe_3B are plotted in Fig. S3. It can be seen that the 3*d* orbitals of Fe contribute significantly when the binding is between Fe and H. When it is between B and H, the *s* and *p* orbitals contribute to different energy ranges. Therefore, the Fe-*d*, B-*s*, and B-*p* orbitals before and after adsorption are all studied. The *s* orbitals of H in adsorbed and gas states are plotted in red line and pink solid fill, respectively. The *d* orbitals of Fe or *s* orbitals of B are both plotted in black and blue lines before and after adsorption. Besides, the *p* orbitals of B are plotted in purple and green lines before and after adsorption. The dotted line in the figure is to show the change of energy width of the orbit. We choose the most representative interaction atoms including Fe6-H2, Fe18-H4, Fe20-H6, B3-H7, B5-H9, and F66-H11. After adsorption, there is a bonding between Fe and H. The *s* states of H shift down to lower energy states, which are further away from the Fermi level. From Fig. S3a-c, H-*s* orbitals keep moving to lower states and then move to higher states according to Fig. S3d-f. This is consistent with the above-mentioned statement that the adsorption energy climbs up through adsorbing the first to the third H_2 and then decline through adsorbing the fourth to the sixth H_2. Therefore, it is deduced that Fe_3B phase tends to be saturated and not so easy to adsorb H_2 after the adsorption of three H_2. According to the PDOS, Fe-3*d* hybridize with the H-*s* orbitals mainly in the range from -8 to -4 eV. There is a significant increase in the orbital width of Fe atoms and this trend becomes more obvious in Fig. S3a-c. Combining with the evidence that B starts to participate in the fourth and fifth H_2 adsorption systems, it is reasonable to believe that hydrogen is only weakly adsorbed at the B sites. The orbitals of B hybridize with that of H, which is not consistent with the small adsorption energies. However, the charge transfers are relatively small and it may be confirmed that hydrogen adsorption is dominated by charge transfer. The obvious hybrid peak appears between the H-*s* orbital and the B-*s* or B-*p* orbital. This orbital hybridization tends to form a covalent bond between H and B.

3. List of Figures and Tables:

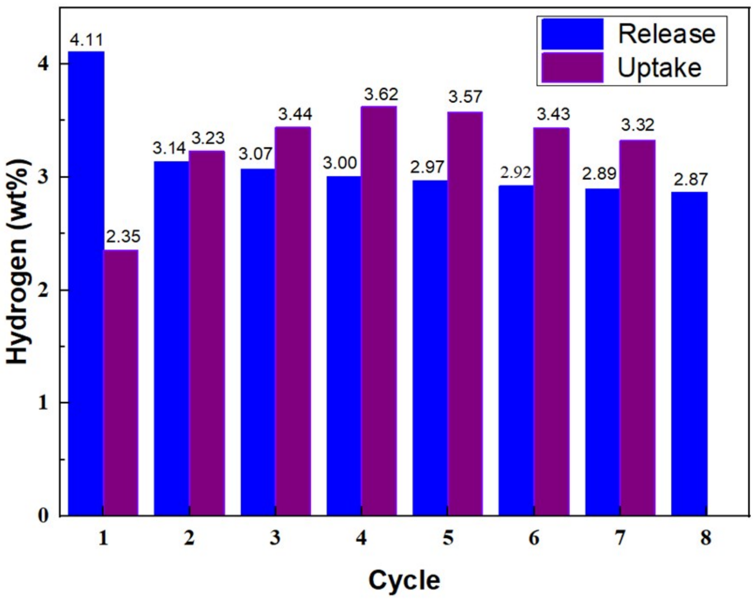

Fig. S1 Hydrogen amount of desorption and absorption for the $LiBH_4$ + MgH_2 system as a function of dehydrogenation and re-hydrogenation cycles.

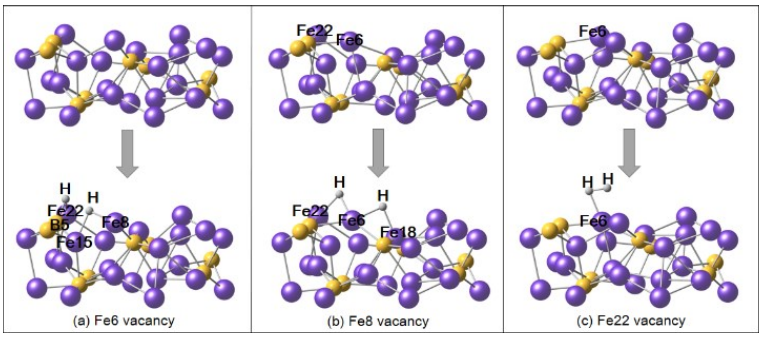

Fig. S2 Optimized geometric structures of H_2 adsorbed on defective Fe_3B.

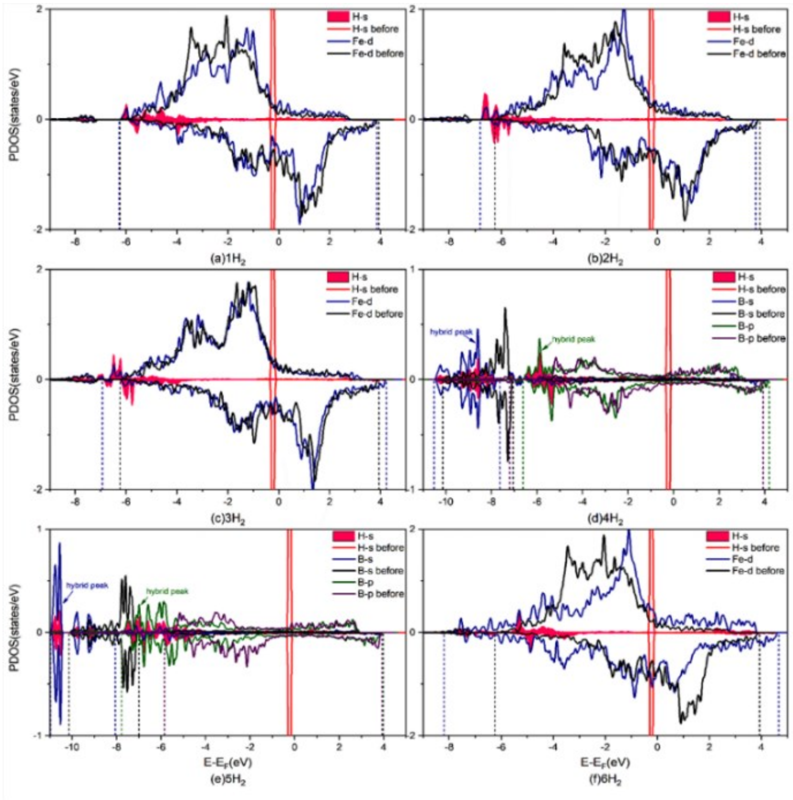

Fig. S3 PDOS profiles of the first to sixth H_2 adsorbed on Fe_3B.

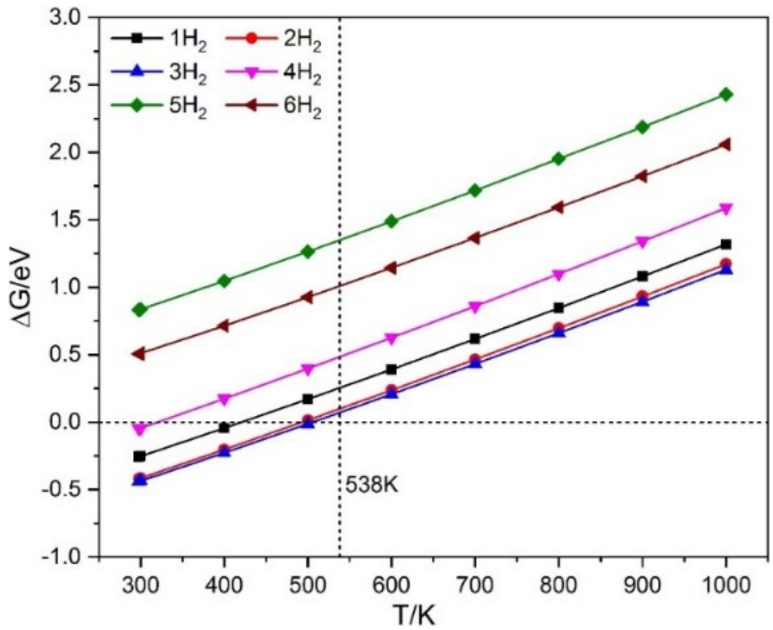

Fig. S4 ΔG profiles of the first to sixth H_2 adsorbed on Fe_3B as a function of temperature.

Table S1 Adsorption energy (E_{ads}, eV), charge variation (Δq, e), and bond length (d, Å) of each H_2 adsorption on Fe_3B.

Number of H_2 (n)	E_{ads} (eV)	Δq_{sub} (e)	Δq_{H2} (e)	d (Å)		
1	-1.00	-0.60	0.62	Fe6-H1 1.68	Fe6-H2 1.67	H1-H2 2.49
2	-1.17	-0.67	0.69	Fe2-H3 1.79	Fe18-H4 1.72	H3-H4 2.92
3	-1.19	-0.66	0.68	Fe10-H5 1.77	Fe20-H6 1.77	H5-H6 5.90
4	-0.87	-0.74	0.76	B3-H7 1.31	Fe6-H8 1.76	H7-H8 5.91
5	0.01	-0.54	0.56	B5-H9 1.34	Fe15-H10 1.68	H9-H10 2.45
6	-0.24	-0.46	0.47	Fe6-H11 1.56	Fe24-H12 1.71	H11-H12 3.01

Table S2 Charge changes of the adsorption sites in the perfect and defective model (Δq, e)

Model / Adsorption Sites	Perfect model	Model with Fe6 vacancy	Model with Fe8 vacancy	Model with Fe22 vacancy
Fe6	-0.16		-0.17	0.12
Fe8	-0.10	0.01		
Fe18			-0.07	
Fe22	-0.12	-0.01	-0.07	
B5		-0.52		

Table S3 Charge changes of all the H and adsorption sites (Δq, e)

Adsorption sites	Δq (e)	Hydrogen atoms	Δq (e)
(a)Fe6	-0.16	(a)H1	0.33
(a)Fe6	-0.16	(a)H2	0.28
(b)Fe2	-0.15	(b)H3	0.36
(b)Fe18	-0.10	(b)H4	0.33
(c)Fe10	-0.17	(c)H5	0.36
(c)Fe20	-0.09	(c)H6	0.32
(d)B3	-0.41	(d)H7	0.46
(d)Fe6	-0.01	(d)H8	0.30
(e)B5	-0.32	(e)H9	0.36
(e)Fe15	-0.02	(e)H10	0.20
(f)Fe6	0.07	(f)H11	0.18
(f)Fe24	-0.02	(f)H12	0.29

Reference

1. R. G. Parr, S. R. Gadre and L. J. Bartolotti, *Proceedings of the National Academy of Sciences*, 1979, **76**, 2522-2526.
2. G. Kresse and J. Furthmüller, *Computational materials science*, 1996, **6**, 15-50.
3. H. Li, W. Chai and G. Henkelman, *Journal of Materials Chemistry A*, 2019, **7**, 23868-23877.
4. K. T. Chan, J. Neaton and M. L. Cohen, *Physical Review B*, 2008, **77**, 235430.
5. G. Kresse and J. Furthmüller, *Physical review B*, 1996, **54**, 11169.
6. G. Kresse and D. Joubert, *Physical review b*, 1999, **59**, 1758.
7. H. Li, K. Shin and G. Henkelman, *The Journal of chemical physics*, 2018, **149**, 174705.
8. H. Li, S. Guo, K. Shin, M. S. Wong and G. Henkelman, *ACS Catalysis*, 2019, **9**, 7957-7966.
9. W. Yang, Z. Gao, X. Liu, X. Ding and W. Yan, *Chemical Engineering Journal*, 2019, **361**, 304-313.
10. W. Yang, Z. Gao, X. Liu, C. Ma, X. Ding and W. Yan, *Fuel*, 2019, **243**, 262-270.
11. L. Gong, J.-J. Chen and Y. Mu, *Physical Chemistry Chemical Physics*, 2017, **19**, 28344-28353.
12. H. J. Monkhorst and J. D. Pack, *Physical review B*, 1976, **13**, 5188.
13. K. T. Chan, J. B. Neaton and M. L. J. P. R. B. Cohen, 2008, **77**, 235430.
14. A. Vojvodic, J. Nørskov and F. Abild-Pedersen, *Topics in catalysis*, 2014, **57**, 25-32.
15. G. Henkelman, A. Arnaldsson and H. Jónsson, *Computational Materials Science*, 2006, **36**, 354-360.
16. O. L. C. Bracho, V. A. Ranea, I. M. Irurzun, R. Imbihl and E. E. Mola, *Chemical Physics Letters*, 2011, **505**, 21-25.
17. P. Cabrera-Sanfelix, *The Journal of Physical Chemistry A*, 2009, **113**, 493-498.